THE ASTROPHYSICAL JOURNAL, 478:614–623, 1997 April 1

A 2000 $M_\odot$ ROTATING MOLECULAR DISK AROUND NGC 6334A

KATHLEEN E. KRAEMER, JAMES M. JACKSON, TIMOTHY A. D. PAGLIONE, AND ALBERTO D. BOLATTO[1]
Astronomy Department, Boston University, 725 Commonwealth Avenue, Boston, MA 02215;
kraemer@fish.bu.edu, jackson@fish.bu.edu, paglione@fish.bu.edu, bolatto@fish.bu.edu
Received 1996 July 19; accepted 1996 October 24

ABSTRACT

We present millimeter and centimeter wave spectroscopic observations of the H II region NGC 6334A. We have mapped the source in several transitions of CO, CS, and NH_3. The molecular emission shows a distinct flattened structure in the east-west direction. This structure is probably a thick molecular disk or torus (2.2 × 0.9 pc) responsible for the bipolarity of the near-infrared (NIR) and radio continuum emission which extends in two "lobes" to the north and south of the shell-like H II region. The molecular disk is rotating from west to east ($\omega \approx 2.4$ km s^{-1} pc^{-1}) about an axis approximately parallel to the radio and NIR emission lobes. By assuming virial equilibrium, we find that the molecular disk contains $\sim 2000\ M_\odot$. Single-component gas excitation model calculations show that the molecular gas in the disk is warmer and denser ($T_k \approx 60$ K, $n \approx 3000$ cm^{-3}) than the gas to the north and south ($T_k \approx 50$ K, $n \approx 400$ cm^{-3}).

High resolution ($\sim 5''$) NH_3 (3, 3) images of NGC 6334A reveal several small (~ 0.1 pc) clumps, one of which lies southwest of the radio continuum shell, and is spatially coincident with a near-infrared source, IRS 20. A second NH_3 clump is coincident with an H_2O maser and the center of a molecular outflow. The dense gas tracers, CS $J = 5 \rightarrow 4$ and $7 \rightarrow 6$, peak near IRS 20 and the H_2O maser, not at NGC 6334A. IRS 20 has a substantial far-infrared (FIR) luminosity $L_{FIR} \sim 10^5\ L_\odot$, which indicates the presence of an O 7.5 star but has no detected radio continuum ($F_{6\ cm} < 0.02$ Jy). The combination of dense gas, a large FIR luminosity and a lack of radio continuum can best be explained if IRS 20 is a protostar. A third clump of NH_3 emission lies to the west of IRS 20 but is not associated with any other molecular or continuum features. The star formation activity in the region has moved west of NGC 6334A to IRS 20 and the H_2O maser position. We suggest that NGC 6334A, IRS 20, and the H_2O maser spot are part of a "protocluster" of stars which is condensing from the massive molecular disk. The similarity between the structure around NGC 6334A and other large ($r \sim 1$ pc), massive ($M \sim 10^3\ M_\odot$), rotating disks (K3-50A and G10.6−0.4) suggests that this may be a common mechanism by which open clusters form.

Subject headings: ISM: H II regions — ISM: individual (NGC 6334A) — ISM: kinematics and dynamics — ISM: molecules — radio lines: ISM — stars: formation

1. INTRODUCTION

NGC 6334 is a southern H II region/star-forming cloud with at least seven sites of active massive star formation ($d = 1.7$ kpc; Neckel 1978). One of these sites of massive star formation, NGC 6334A,[2] has a shell-like morphology in 6 cm radio continuum emission (Rodríguez, Cantó, & Moran 1982), with fainter radio emission extending in bipolar lobes to the north and south (Rodríguez, Cantó, & Moran 1988, hereafter RCM88). NGC 6334A also has a bipolar morphology in near-infrared continuum emission (Harvey, Hyland, & Straw 1987), with extended nebulosity nearly coincident with the radio lobes. *IRAS* HIRES 12 and 25 μm data show double lobes to the north and south of NGC 6334A as well (Fig. 1). Also associated with NGC 6334A are a CO "hot spot" (Dickel, Dickel, & Wilson 1977; Phillips, de Vries, & de Graauw 1986; this work), a Herbig-Haro–like object (Gyulbuaghian, Glushkov, & Denisyuk 1978; Bohigas 1992), high-velocity H_2O masers (Rodríguez et al. 1980; Moran & Rodríguez 1980), and [C II] 158 μm, [O I] 145 μm, and [O I] 63 μm emission (Kraemer et al. 1994). A far-infrared continuum source ($\lambda \approx 70$ μm, McBreen et al. 1979; Loughran et al. 1986) coincides with the radio source. Two unresolved near-infrared (2.2 μm) sources (IRS 19 and IRS 20) are located between the extended continuum lobes (Harvey et al. 1987; Harvey & Gatley 1983, hereafter HG83).

RCM88 suggested that the H II region is confined in the east-west direction by a flattened structure of gas and dust, which would allow radiation to escape easily only to the north and south. There is some indirect evidence in support of this suggestion. A flattened dust structure oriented with its major axis in the east-west direction is implied by the elongated morphology seen in a map of 100 μm optical depth (HG83). Moreover, De Pree et al. (1995) found an east-west velocity gradient in the H76α recombination line which they suggest arises from the ionized portion of a rotating accretion disk.

We have imaged NGC 6334A in several millimeter and centimeter molecular lines in order to examine the distribution and physical conditions of the molecular gas. The CO lines give the overall morphology of the gas, while the CS lines show where the dense gas lies. The NH_3 (3, 3) image reveals the small-scale structure of the warm dense molecular gas near the continuum sources. We find that NGC 6334A is surrounded by a massive, flattened, rotating structure of molecular gas, just as RCM88 proposed. The emission from the dense gas tracers does not peak at NGC 6334A. Instead, they peak to the west, near the infrared source IRS 20 and an H_2O maser, which are probably protostars. Apparently, the star formation activity has moved

[1] Departamento de Astronomía, Universidad de la República, Montevideo, Uruguay.

[2] After the nomenclature of Rodríguez et al. (1982). NGC 6334A is spatially coincident with the FIR source NGC 6334IV (McBreen et al. 1979).

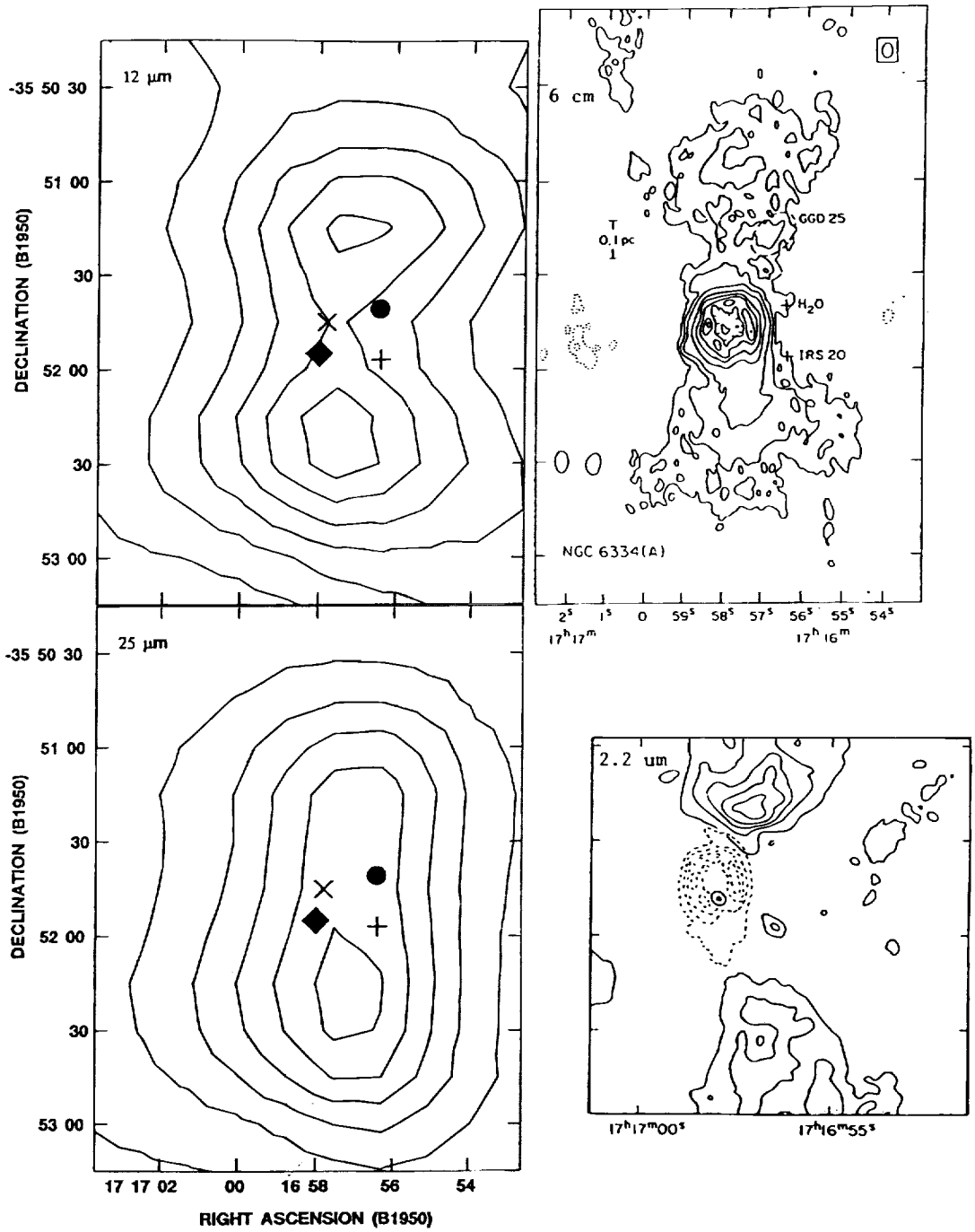

FIG. 1.—Continuum emission at NGC 6334A: (*a*) 12 μm *IRAS* HIRES image, peak = 1.4 kMJy sr^{-1}, contours at 200 MJy sr^{-1} intervals, lowest contour 300 MJy sr^{-1}. Positions of additional features are marked: 6 cm position (*cross*; Rodríguez et al. 1982), FIR peak (*filled diamond*; McBreen et al. 1979), IRS 20 (*plus*; Harvey et al. 1987), and the H_2O maser (*filled circle*; Rodríguez et al. 1980; RCM88). (*b*) 25 μm *IRAS* HIRES image, peak = 9.5 kMJy sr^{-1}, contours at 800 MJy sr^{-1} intervals. (*c*) 6 cm radio image (RCM88). (*d*) *K*-band image (HG83).

away from NGC 6334A. We suggest that a "protocluster" of stars is condensing out of the rotating cloud fragment.

2. OBSERVATIONS

We used the Caltech Submillimeter Observatory to map NGC 6334 in the CO $J = 2 \rightarrow 1$ and $3 \rightarrow 2$, the ^{13}CO $2 \rightarrow 1$, and the CS $5 \rightarrow 4$ and $7 \rightarrow 6$ transitions. The CO $2 \rightarrow 1$, ^{13}CO $2 \rightarrow 1$, and CS $5 \rightarrow 4$ observations were made on 1993 August 7–13. The CO $3 \rightarrow 2$ and CS $7 \rightarrow 6$ lines were observed simultaneously in dual-sideband mode, with one line in each sideband, on 1994 June 29–July 1. The facility 230 and 345 GHz SIS receivers were used with the AOS backend (500 MHz bandwidth, 1024 channels). We imaged the cloud in CS $3 \rightarrow 2$ at the NRAO 12 m telescope[3] at Kitt Peak on 1995 October 7. The λ2 mm SIS receiver was used with the analog filterbank in the 256 channel, 1000 kHz channel^{-1} setting. All maps employed the "on-the-fly" mapping technique. At the CSO, individual grids (9 × 13

[3] The 12 m and VLA are operated by the National Radio Astronomy Observatory, which is operated by Associated Universities, Inc., under a cooperative agreement with the National Science Foundation.

and 13 × 19 pixels for 1993 and 1994, respectively) were mosaicked to create the larger maps. At the NRAO 12 m, a 64 × 64 pixel grid was observed. A single spectrum of CO 1 → 0 emission toward NGC 6334A was obtained with the NRAO 12 m on 1995 April 5. Observational parameters are summarized in Table 1.

The CSO data were processed with the CLASS and GreG packages and the NRAO data with the AIPS package. For calibration we used the standard chopper wheel method (Ulich & Haas 1976). Pointing was established through observations of Jupiter and varied by less than 5″. The spectra were individually inspected and linear or parabolic baselines were removed as necessary. All data are presented on the T_{mb} scale, that is, $T_{mb} = T_A^*/\eta_{mb}$ (Table 1). Intensities are estimated to be accurate to ≈30%.

The NH_3 (3, 3) observations were made with the VLA[3], in the DnC array, on 1993 October 19 and 21. The NH_3 (3, 3) data were edited and calibrated in AIPS. The "pseudo-continuum" data, from the "channel 0" (the central 75% of the passband) were CLEANed and self-calibrated. A uniformly weighted image was made in order to examine the continuum at high angular resolution. The continuum self-calibration solutions were then applied to the u, v line data. These data were used to produce a naturally weighted image cube, with a 30 kλ taper applied. Emission-free channels were averaged and subtracted from the data to produce a data cube which contained only line emission.

3. THE MOLECULAR DISK

3.1. *Morphology*

The presence of a flattened structure of gas and dust was suggested by RCM88 to attenuate the radiation from the central star and to inhibit the expansion of the H II region in the east-west direction. Increased opacity in an east-west structure in the 100 μm optical depth map (HG83) provides indirect evidence in support of their suggestion.

Our new observations show directly that the CO and CS emission is arranged in a flattened 2.2 × 0.9 pc structure (Fig. 2). In every transition, each of which is sensitive to different molecular gas densities, the emission is elongated in an east-west direction. The orientation of the major axis (P.A. ≈ 90°) of the molecular gas emission varies by less than 10° among the various CO and CS lines. The FWHM axial ratio (Table 2) of the CO integrated intensity ranges from 1.6 for the CO 3 → 2 emission to 2.5 for that of ^{13}CO 2 → 1. Along the minor (north-south) axis, the CS 3 → 2 emission is barely resolved, and the CS 5 → 4 and 7 → 6 emission are unresolved. Thus, the CS axial ratio of ∼2 is a lower limit, and the dense gas, traced by the CS emission, may be more flattened than the more diffuse gas, traced by CO. A flattened structure similar to the molecular gas structure we observe toward NGC 6334A arises naturally upon

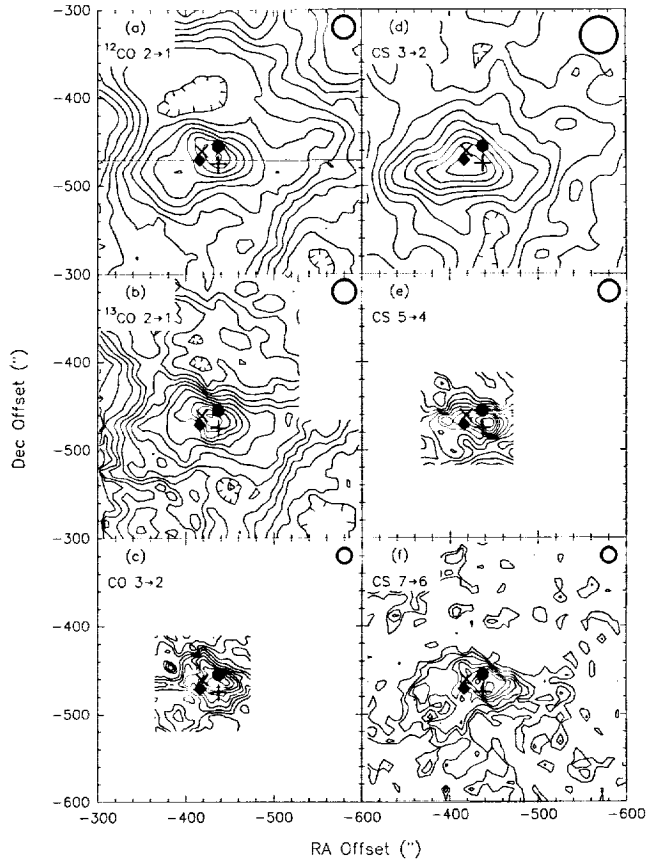

FIG. 2.—Molecular emission at NGC 6334A. The (0, 0) position is $\alpha = 17^h17^m32^s$, $\delta = -35°44'04''$, the position of NGC 6334 F. (*a*) CO 2 → 1, peak integrated intensity = 708 K km s^{-1}, contours are at 50 K km s^{-1} intervals. (*b*) ^{13}CO 2 → 1, peak = 212 K km s^{-1}, contours are at 15 K km s^{-1} intervals. (*c*) CO 3 → 2, peak = 743 K km s^{-1}, contours are at 50 K km s^{-1} intervals. (*d*) CS 3 → 2, peak = 97 K km s^{-1}, contours are at 10 K km s^{-1} intervals; (*e*) CS 5 → 4, peak = 57 K km s^{-1}, contours are at 5 K km s^{-1} intervals; (*f*) CS 7 → 6, peak = 88 K km s^{-1}, contours are at 10 K km s^{-1} intervals. Spectra along the horizontal line in (*a*) were fitted with Gaussian profiles for the velocity field diagram (Fig. 3)

TABLE 1

OBSERVATIONAL PARAMETERS

Species	Transition	Frequency (GHz)	Velocity Resolution (km s^{-1})	Beam (arcsec)	Telescope[a]	η_{mb}	T_{sys} (K)
CO	$J = 1 \rightarrow 0$	115.271	2.60	53	KP	0.55	900
	$J = 2 \rightarrow 1$	230.538	0.74	26	CSO	0.74	800
	$J = 3 \rightarrow 2$	345.796	0.49	17	CSO	0.62	4100
^{13}CO.....	$J = 2 \rightarrow 1$	220.399	0.78	27	CSO	0.74	1750
CS.....	$J = 3 \rightarrow 2$	146.969	2.04	42	KP	0.55	650
	$J = 5 \rightarrow 4$	244.936	0.70	24	CSO	0.74	1000
	$J = 7 \rightarrow 6$	342.883	0.49	17	CSO	0.74	4100
NH_3	(J, K) = (3,3)	23.870	2.45	6.6 × 5.1[b]	VLA		
	1.3 cm continuum	23.870	...	2.3 × 2.0[c]	VLA		

[a] KP: NRAO 12 m at Kitt Peak; CSO: Caltech Submillimeter Observatory; VLA: Very Large Array.
[b] Natural weighting with a 30 kλ taper.
[c] Uniform weighting.

TABLE 2

PROPERTIES OF THE MOLECULAR GAS STRUCTURE

Line	Size[a] (arcsec × arcsec)	r_h[b] (pc)	Δv (km s^{-1})	M ($M_\odot$)
CO 2 → 1	126 × 54	1.1	3.9	2400
^{13}CO 2 → 1.....	96 × 38	0.8	2.5	730
CO 3 → 2.....	39 × 24	0.3	2.4	280
CS 3 → 2.....	86 × 46	0.7	2.6	710
CS 5 → 4.....	42 × 15	0.4	2.3	270
CS 7 → 6.....	34 × 17	0.3	1.5	90

[a] Semimajor axis by semiminor axis at the half-power level of the integrated intensity.

[b] At a distance of 1.7 kpc (Neckel 1978), 1′ ~ 0.5 pc.

the gravitational collapse of rotating clouds (cf. Boss 1987; Mestel 1965).

3.2. *Kinematics*

If the flattened structure of molecular gas arose from the collapse of a rotating cloud, we expect to see evidence of rotation in the kinematics of the gas. We fit Gaussian line profiles to the spectra along $\Delta\delta \approx -471''$[4] across the structure (Fig. 2*a*), which are the spectra nearest to the major axis, and along $\Delta\alpha \approx -439''$, near the minor axis. Figure 3*a* shows the central velocity from the Gaussian fits versus position across the molecular structure at $\Delta\delta \approx -471''$. In each transition, the velocity field shows a clear linear gradient of 2.4 km s^{-1} pc^{-1} along the major axis of the molecular emission. There is no systematic change along the minor axis from the average central velocity $v_{LSR} \approx -3$ km s^{-1}. Figure 3*b* shows the position-velocity diagram of the CO 2 → 1 emission, which again shows the linear gradient. The gradient in the position-velocity diagram also shows that Gaussian profiles approximate the line shapes well. An east-west velocity gradient, that is, across the major (east-west) axis of the structure, is strong evidence that the molecular gas is rotating around a north-south axis. The combination of the linear velocity gradient, the elongation of the molecular emission, and the bipolarity of the diffuse continuum emission in a perpendicular direction leads us to conclude that the structure is a rotating disk or torus of molecular gas and dust, with an angular velocity of $\omega \approx 2.4$ km s^{-1} pc^{-1}. This rotating molecular disk is the structure predicted by RCM88 which allows the continuum emission to escape only perpendicular to the structure.

Unlike the velocity gradient seen on small scales ($\lesssim 30''$ from NGC 6334A) in hydrogen recombination lines (De Pree et al. 1995), in which the velocity increases to the northwest, the velocity of the molecular lines increases to the east. Central line velocities of the spatially integrated H76α and H92α profiles are $v_{LSR} \approx -0.1$ and -0.32 km s^{-1}, respectively, and the velocity gradient across the H II region is $\approx$75 km s^{-1} pc^{-1} from southeast to northwest (P.A. $\approx -60°$; De Pree et al. 1995). De Pree et al. interpret this gradient as the combination of a north-south bipolar outflow and a rotating ionized disk with position angle P.A. $\approx -90°$. In contrast, the average central velocity of the molecular emission lies at $v_{LSR} \approx -3.0$ km s^{-1} and has a position angle of P.A. $\approx +90°$. Clearly the motions of the ionized gas are not coupled to the rotation of the molecular disk. This type of peculiar behavior, in which the ionized and molecular components seem to rotate in opposite directions, has been reported in at least one other source, G34.3+0.2 (Garay & Rodríguez 1990), but there is no theoretical explanation that we are aware of. We note that in NGC 6334A, the reddest H76α emission (De Pree et al.

[4] Offsets are with respect to the (0, 0) position at $\alpha = 17^h17^m32^s$, $\delta = -35°44'04''$, the position of NGC 6334F.

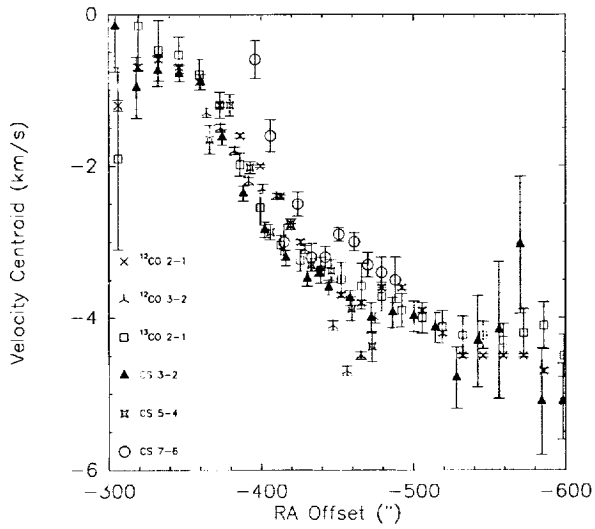

FIG. 3*a*

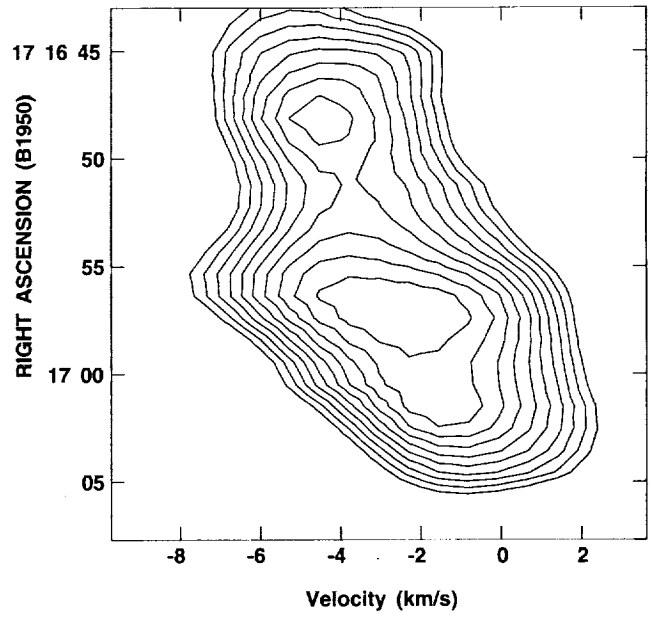

FIG. 3*b*

FIG. 3.—(*a*) Velocity field diagram for the millimeter molecular lines. Velocities are taken from single Gaussian fits to each spectrum along a line of constant declination ($\Delta\delta \approx -471''$; Fig. 1), approximately coincident with the major axis of the molecular disk. Note the smooth gradient across the disk. Error bars are formal errors to the Gaussian fits. (*b*) Position-velocity diagram of the CO 2 → 1 emission across $\Delta\delta \approx -471''$, the major axis of the disk (*horizontal line* in Fig. 2*a*). The coverage in right ascension is the same as in Fig. 3*a*. Contour levels are at 5% intervals of the 53 K peak (average) temperature; the lowest contour is at 50%. The higher velocity emission seen at $\alpha \approx 17^h16^m56^s$ is from the molecular outflow associated with the H_2O maser (§ 5.2).

1995) appears coincident with NH_3 (3, 3) emission at the H II region (Fig. 4). This ionized gas may be the photoionized edge of the dense gas clump, not part of a rotating ionized disk. However, the apparent increase of the ionized gas velocity to the northwest, as opposed to the increase of the molecular gas velocity to the east, remains puzzling.

3.3. *Mass*

If the virial theorem holds, the mass of the disk can be estimated in each of the molecular transitions by

$$M \simeq \frac{r_h(0.5\,\Delta v)^2}{0.4G},$$

where M is the mass and G is the gravitational constant (Binney & Tremaine 1987). The median radius, r_h, which encloses half of the mass, was calculated by estimating the size of the major axis at the half-power contour of the integrated intensity maps. The numerical factor, 0.4, accounts for the difference between r_g, the radius enclosing all the gravitational mass, and r_h, the median radius. The velocity change across the major axis, Δv, is determined by linear regression from the velocity field (Fig. 3*a*).

Because of the high axial ratio in the dense gas tracers, we assume the disk is edge-on in the calculations of virial mass. If the disk is inclined by an inclination angle i, then the derived virial masses must by corrected by $(\sin i)^{-2}$. By considering the case of a thin disk, we can place a limit on the inclination angle. If the disk were infinitely thin, then the observed thickness of the minor axis, $r_{\rm minor} = 0.9$ pc, would be due entirely to i. The observed axial ratio sets a limit on i: $\sin i \gtrsim (0.9/2.2)$ or $65° < i < 90°$. For the lowest possible inclination, $i \approx 65°$, the virial mass increases by less than 20%. Therefore, we conclude that inclination effects on the mass derivation are unimportant.

The results of the mass calculations are given in Table 2. The virial masses derived vary from 90 $M_\odot$ for the CS $7 \rightarrow 6$ emission to 2400 $M_\odot$ for that of CO $2 \rightarrow 1$. If the rotational velocities were due primarily to a central, condensed core of material, the calculated mass would be similar from each transition, not increasing. Also, the velocity field is linear across the disk, which is consistent with solid body rotation.

The virial mass we derive from the CO $2 \rightarrow 1$ emission of $M_{\rm vir} = 2.4 \pm 1.1 \times 10^3\ M_\odot$ is in excellent agreement with the molecular mass, $M_{\rm H_2} = 2.2 \pm 1.4 \times 10^3\ M_\odot$, obtained by assuming a CO-to-H_2 conversion factor of $N({\rm H_2})/I_{1\rightarrow 0}({\rm CO}) = 2.2 \times 10^{20}$ cm^{-2} (K km s^{-1})$^{-1}$ (Combes 1991) and applying it to the mean CO $(2 \rightarrow 1)$ integrated intensity (averaged over a similar area). The uncertainty in the virial mass derivation is dominated by the uncertainty in Δv from the linear fit to the velocity field. For the molecular mass, the 30% uncertainty in the intensity calibration and an estimated 30% uncertainty in the CO-to-H_2 conversion factor contribute equally to the total uncertainty. Our use of CO $2 \rightarrow 1$ instead of CO $1 \rightarrow 0$ is unlikely to be problematic since the integrated intensity ratio in a 55″ beam toward NGC 6334A is CO $(2 \rightarrow 1)$/CO $(1 \rightarrow 0) \approx 1$, which indicates the CO is optically thick. These masses are slightly larger than that measured by Dickel et al. (1977), $M_{\rm H_2} \sim 10^3\ M_\odot$. Their measurements, however, were made at least 30″ southeast of our CO peak, which probably accounts for the difference.

To summarize, we find a large (2 pc diameter), massive (2000 $M_\odot$), rotating disk or torus of molecular gas surrounding NGC 6334A. The disk lies nearly edge-on in the east-west plane, is perpendicular to the lobes of radio and infrared continuum emission, and rotates about an axis parallel to the extended continuum emission. This rotating molecular disk is the structure of gas and dust which, based on the bipolarity of the continuum emission and the elongated 100 μm opacity structure, RCM88 predicted was present.

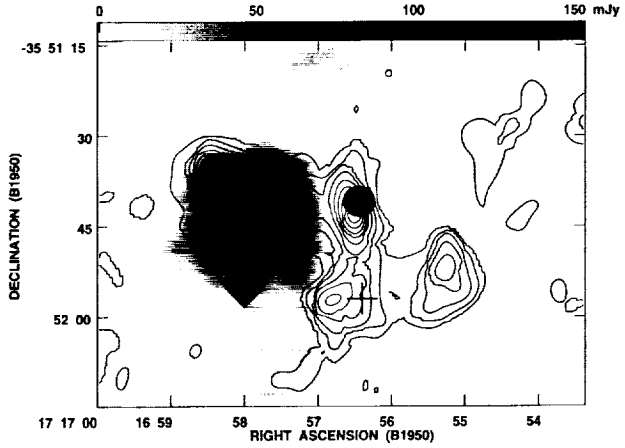

FIG. 4.—NH_3 (3, 3) emission from NGC 6334A (contour interval is 10% of the 0.82 Jy beam^{-1} km s^{-1} peak), superposed on the 23 GHz continuum emission (peak flux = 150 mJy beam^{-1}). Positions of additional features are marked: 6 cm position (*cross*; Rodríguez et al. 1982), FIR peak (*filled diamond*; McBreen et al. 1979), IRS 19 and 20 (*plus*; Harvey et al. 1987), and the H_2O maser (*filled circle*; Rodríguez et al. 1980; RCM88).

4. RELATION BETWEEN MOLECULAR GAS AND CONTINUUM EMISSION

4.1. *Physical Conditions*

In the CO $2 \rightarrow 1$ line, the molecular gas apparently *avoids* the continuum lobes, as two distinct bubbles in the emission coincide with the radio continuum lobes (Fig. 5). RCM88 suggested that the lobes of radio continuum radiation are caused by thermal emission from ionized gas and that the NIR emission is detectable because of lower extinction at the lobe positions relative to the surrounding region. We can test this hypothesis by determining the physical conditions of the molecular gas in the disk and toward the continuum lobes. Qualitatively, comparison of the CO $2 \rightarrow 1$ line emission with the ^{13}CO $2 \rightarrow 1$ emission (Fig. 6) shows that the CO opacity is indeed lower toward the lobes. Ratios of $T_{mb}({\rm CO})/T_{mb}(^{13}{\rm CO})$ indicate that $\tau_{\rm CO} \approx 40$ in the disk, as opposed to $\tau_{\rm CO} \approx 15$ toward the continuum lobes.

A more detailed, multiline analysis confirms this qualitative result. We performed single-component model calculations of non-LTE CO excitation to determine the physical conditions of the molecular gas. The model assumes that the emission originates in unresolved, homogeneous, spherical clumps. A photon escape probability function was included to account for the radiative excitation of optically thick lines (see Stutzki & Winnewisser 1985, and references therein). We modeled the emission from the first 11 levels of CO by varying the kinetic temperature, CO column density per velocity interval, and H_2 density until the best χ^2 fit to the data was achieved. We used the collision rates of Flower & Launay (1985). We assumed that the beam-filling factor,

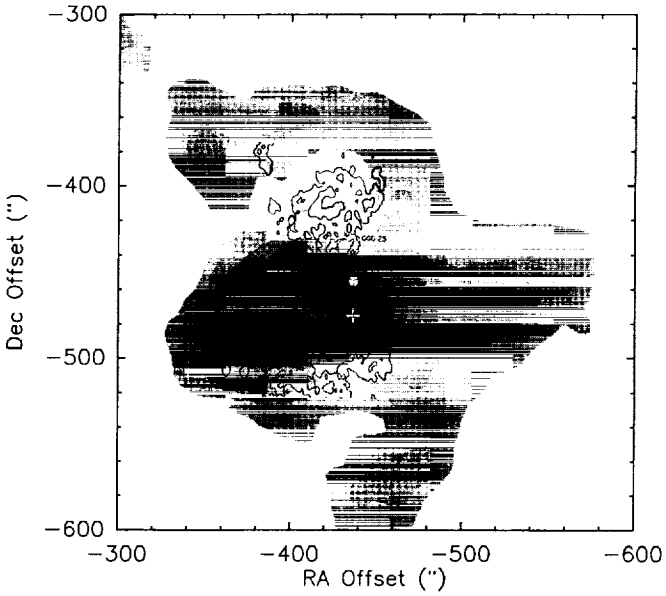

FIG. 5.—6 cm radio continuum emission (*contours*;RCM88) superposed on the CO 2 → 1 integrated intensity (*gray scale*, 340–700 K km s^{-1}). Note the bubbles of decreased CO emission to the north and south of the peak near NGC 6334A coincide with the diffuse continuum emission.

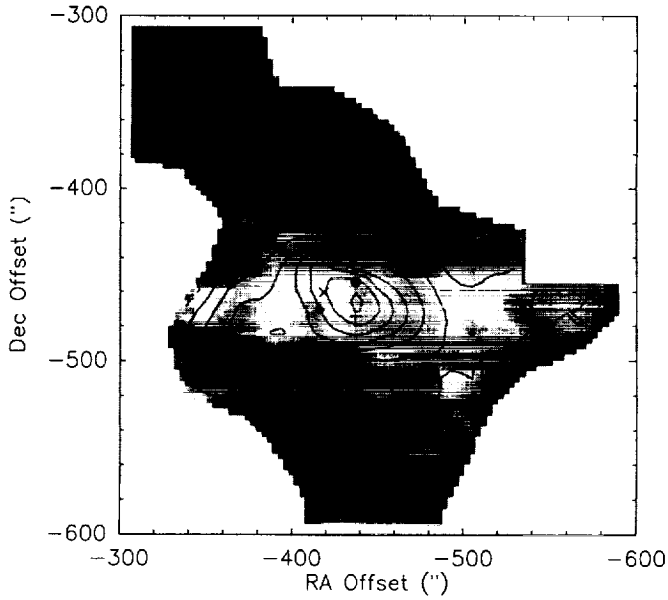

FIG. 6.—Map of optical depth as traced by the CO/^{13}CO 2 → 1 integrated intensity ratio (*gray scale*), superposed on the CO 2 → 1 integrated intensity map (*contours*).

the fraction of the beam area covered by emission ($\phi = T_{mb}/T_{\rm intrinsic}$), was the same for each transition. A CO/^{13}CO abundance ratio of 60 was adopted. We did not include dust continuum emission, as it has negligible effect on low J CO excitation (cf. Jackson et al. 1995). Observed line parameters and the model results toward NGC 6334A, the northern lobe, located at $(\Delta\alpha, \Delta\delta) \approx (-410'', -415'')$, and the southern lobe, $(\Delta\alpha, \Delta\delta) \approx (-417'', -555'')$, are summarized in Table 3.

By assuming a [CO]/[H_2] abundance ratio of 8×10^{-5} (Frerking, Langer, & Wilson 1982) and multiplying the derived column density per velocity interval by the line width (Table 3), we find that the molecular hydrogen column density toward NGC 6334A is $N_{H_2} \sim 1.3 \times 10^{23}$ cm^{-2}. The hydrogen column densities toward the northern and southern lobes are only $N_{H_2} \sim 4 \times 10^{22}$ cm^{-2} and $N_{H_2} \sim 9 \times 10^{22}$ cm^{-2}, respectively. This confirms our qualitative estimate that the opacity in the disk is higher than the opacity toward the continuum lobes. The lower column density toward the lobes supports the explanation of RCM88 that the diffuse NIR continuum radiation is detectable because of lower opacity in the lobes as compared to that within the molecular disk. Further, the column density toward the southern lobe is roughly a factor of 2 higher than that toward the northern lobe, a result consistent with the suggestion of higher extinction toward the southern lobe (RCM88).

If the expansion of the H II region is inhibited in the east-west direction by the molecular disk, the molecular gas in the disk must be denser than the surrounding gas. Further, when a cloud fragment collapses, as we propose the molecular disk has done, the density will increase as compared to density of the ambient parent cloud. Indeed, we find that the hydrogen volume density in the molecular disk is approximately 1 order of magnitude higher than that toward the lobes. This density enhancement is entirely consistent with both the confinement of the H II region and

TABLE 3

CO LINE PARAMETERS

Parameters	NGC 6334A (−416″, −471″)[a]	Northern Lobe (−410″, −415″)	Southern Lobe (−417″, −555″)
T_{mb} (K):			
CO 1 → 0	41	...	...
CO 2 → 1	58	36	40
CO 3 → 2	49	26	30
^{13}CO 2 → 1	27	6	14
CO (2 → 1)/CO (1 → 0)[b]	1.4	...	...
CO (3 → 2)/CO (2 → 1)	0.8	0.7	0.8
(^{12}CO 2 → 1)/(^{13}CO 2 → 1)	3.7	5.0	4.7
Model Results:			
T_k (K)	60	50	50
log n (cm^{-3})	3.3–3.8	2.7	2.5
log ($N_{CO}/\Delta v$) [cm^{-2} (km s^{-1})$^{-1}$]	17.9–18.1	17.7	18.1
log N_{H_2} (10^{22} cm^{-2})	13	4	9

[a] The (0, 0) position is $\alpha = 17^h17^m32^s$, $\delta = -35°\,44'\,04''$, the position of NGC 6334F.

[b] Integrated intensities were convolved to 55″ (CO 1 → 0 resolution) prior to the ratios.

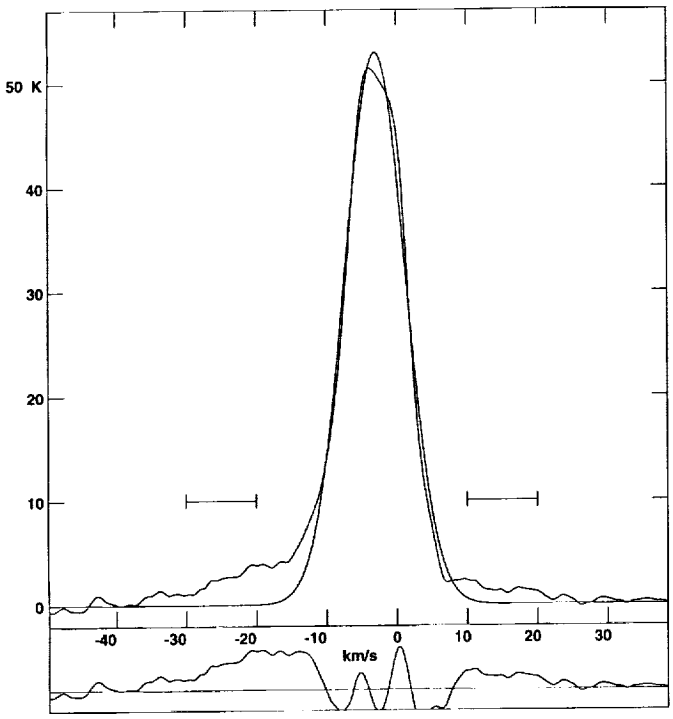

FIG. 7a

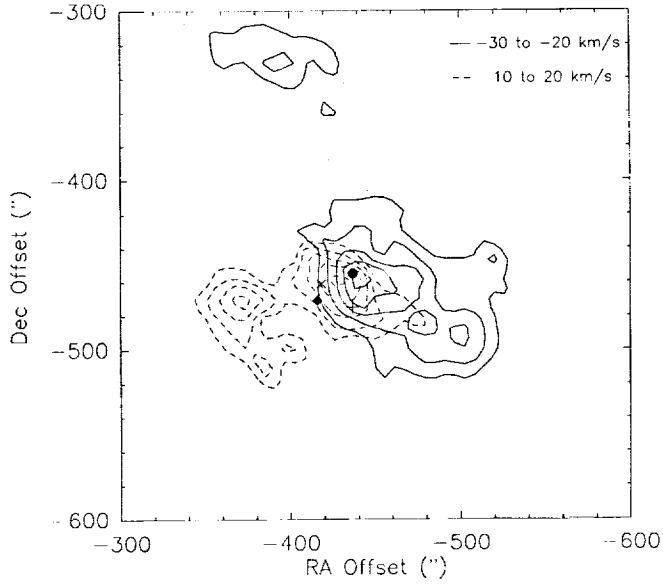

FIG. 7b

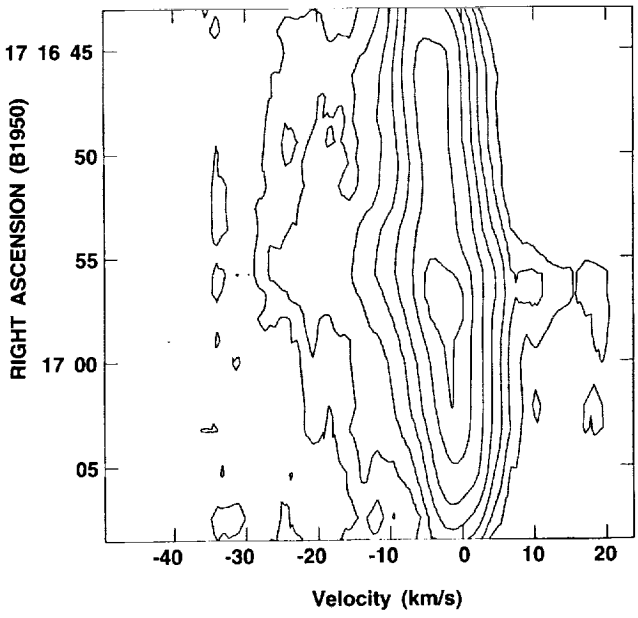

FIG. 7c

FIG. 7.—(*a*) CO 2 → 1 spectrum toward the H_2O maser position (−439, −457), with the Gaussian model fit and residuals. Residuals are on the same scale but are offset for clarity. Horizontal lines at 10 K show the velocity range over which the emission was integrated to produce Fig. 7*b*. (*b*) Contour map of the integrated intensity of the CO 2 → 1 line wings. The redshifted emission (*dashed line*) is integrated from 10–20 km s^{-1}, and the blueshifted emission (*solid line*) is integrated from −30 to −20 km s^{-1}. Note that the outflow is centered on the position of the H_2O maser (*filled circle*). (*c*) Position-velocity diagram centered at the H_2O maser position ($\delta = -35°51'40''.4$). Note the high-velocity emission at $\alpha \approx 17^h16^m56^s$.

with our scenario of a rotating molecular disk which condensed out of the parent cloud.

The CS emission was also modeled, but no valid solutions were found. That is, χ_ν^2, the reduced χ^2, was never above the 5% confidence level. The CO model solutions, for comparison, had χ_ν^2 confidence levels of 55%–85%. We conclude that the single-component model, while valid for the CO emission, does not adequately describe the CS emission. A two-component model, with a small, dense component embedded in an extended, diffuse component, might better describe the CS observations of NGC 6334A.

In fact, large-scale mapping of the entire NGC 6334 complex suggests that the CS 3 → 2 emission and the CS 5 → 4 and 7 → 6 emission indeed trace distinct gas components (Kraemer & Jackson 1997). The CS 5 → 4 and 7 → 6 emission appear only near the active star formation

sites. Apparently these lines specifically trace dense star-forming cores in NGC 6334. On the other hand, the CS $3 \rightarrow 2$ emission is more extended, similar to the CO $2 \rightarrow 1$ morphology. Thus, the CS $3 \rightarrow 2$ emission may be associated with more diffuse gas than the gas traced by CS $5 \rightarrow 4$ and $7 \rightarrow 6$ emission. This is not unexpected, as the critical density of CS $3 \rightarrow 2$ is 13 times smaller than that for CS $7 \rightarrow 6$. Unfortunately, a two-component model has more free parameters than we currently have observables. Further observations of CS isotopes or different CS transitions are needed to properly constrain a two-component model.

5. YOUNG STELLAR OBJECTS NEAR NGC 6334A

5.1. *IRS 20*

Two unresolved IR continuum sources, IRS 19 and 20 (Harvey et al. 1987) (also known as IRS 2 and 3; HG83) lie between the NIR and radio continuum lobes (Fig. 1*c*). IRS 19 coincides with the southern rim of the radio shell, where there is a gap in the radio emission, and is probably associated with the radio source. IRS 20, on the other hand, lies $\sim 20''$ west-southwest of IRS 19 (Fig. 4), just past the edge of the H II region. The two sources are strong at 20 μm (HG83) but not at *J*, *H*, or *K* bands. Indeed, IRS 20 was not even detected at *J* or *H* band ($J > 16.2$, $H > 14.0$; Harvey et al. 1987).

A clump of NH_3 (3, 3) emission, which traces warm, dense gas, coincides with the position of IRS 20 (Fig. 4). The virial mass of this clump is $M_{vir} \approx 80\ M_\odot$. Additionally, a number of other tracers of dense or photodissociated gas are associated with IRS 20. For instance, the CS $5 \rightarrow 4$ and $7 \rightarrow 6$ emission, which are sensitive to densities of $n \gtrsim 10^6$ cm^{-3}, peak not at NGC 6334A but instead at IRS 20 to within the positional errors (Figs. 2*e* and 2*f*). [C II] 158 μm emission, which traces photodissociated gas, is enhanced to the west of NGC 6334A, toward IRS 20, and the [O I] 145 μm emission peak is also coincident with IRS 20 (Kraemer et al. 1994). The association of photodissociated gas with IRS 20 is somewhat puzzling, as IRS 20 is not a radio source (Fig. 4). In order to photodissociate CO and photoionize carbon without photoionizing hydrogen, 15 B1 zero-age main sequence (ZAMS) stars (Panagia 1973) are needed in a region ≈ 0.04 pc across to be consistent with the observed luminosity ($L_{IR} \approx 8 \times 10^4\ L_\odot$; HG83). This required stellar density seems unreasonably high, and we suggest that the [C II] 158 μm and [O I] 145 μm emission are probably due to UV radiation escaping from the H II region. However, the infrared luminosity is far too high for IRS 20 to be merely a clump of gas illuminated by NGC 6334A. If we again assume a size of $r \approx 0.02$ pc, the size of the NH_3 clump, and a projected distance of at least 0.2 pc from NGC 6334A, IRS 20 intercepts less than 2% of the radiation from NGC 6334A. The infrared luminosities of IRS 19, which is almost certainly the exciting source for NGC 6334A, and IRS 20 are both $L_{IR} \sim 10^5\ L_\odot$ (HG83). Clearly, IRS 20 must be self-luminous, and the CS and NH_3 trace dense circumstellar gas surrounding IRS 20.

IRS 20 has an infrared luminosity of $L_{IR} \approx 8 \times 10^4\ L_\odot$, which requires a ZAMS star of O 7.5 (HG83). However, no radio emission has been detected from IRS 20 ($F_{6\ cm} < 0.02$ Jy; RCM88), which puts a limit of B1 on the ZAMS spectral type. The combination of warm, dense gas, with high IR luminosity but no radio emission is exactly what is expected from a protostar. Thus, the evidence from our molecular gas observations supports the view (Harvey et al. 1987; RCM88) that IRS 20 is a site of active star formation near NGC 6334A.

5.2. H_2O *Maser*

Another NH_3 (3, 3) clump, $M_{vir} \approx 300\ M_\odot$, coincides with an H_2O maser position (RCM88; Rodríguez et al. 1980) approximately 15″ north of IRS 20 and 20″ west of the H II region (Fig. 4). The CO $2 \rightarrow 1$ and $3 \rightarrow 2$ emission both show extended line wings, indicative of a molecular outflow, toward the H_2O maser position (Fig. 7*a*). In the CO $2 \rightarrow 1$ emission, the red wings (10–20 km s^{-1}) and blue wings (-20 to -30 km s^{-1}) separate into distinct lobes centered on the H_2O maser position (Fig. 7*b*). The outflow can also be seen in the position-velocity diagram (Fig. 7*c*) at $\alpha \approx 17^h16^m56^s$. We interpret these lobes as a molecular outflow centered on the H_2O maser. The gas in the outflow is at significantly bluer ($v_{LSR} \lesssim -20$ km s^{-1}) or redder ($v_{LSR} \gtrsim 10$ km s^{-1}) velocities than the rotational velocities of the disk. Removing the contribution of the rotating disk from the postition-velocity diagram leaves the high-velocity gas at $\alpha \approx 17^h16^m56^s$, with a much steeper velocity gradient. The combination of warm, dense gas with an H_2O maser and a molecular outflow, both signposts of star formation, indicates that this molecular clump may be yet another site of active star formation in the NGC 6334A area. The lack of IR emission, however, suggests that this source may be either less luminous or more deeply embedded than the IRS 20 protostar.

5.3. *The Westernmost* NH_3 *Clump*

A third clump of NH_3 (3, 3) emission, $M_{vir} \approx 80\ M_\odot$, $\sim 15''$ west of IRS 20, does not seem to be associated with any other molecular features. Also, there is no detected radio (RCM88; this work) or infrared (HG83; Harvey et al. 1987) continuum emission at this location. Apparently, this clump of dense gas has not yet collapsed to form a protostar. However, it does lie to the west of IRS 20, which is the direction in which star formation seems to be spreading from NGC 6334A. We suggest that although not currently active, this NH_3 clump may be the next site of star formation within the molecular disk.

6. CONDENSATION OF A PROTOCLUSTER?

Molecular disks or toroids have long been thought to be the focusing mechanism of bipolar molecular outflows (e.g., Torrelles et al. 1983; Shu et al. 1993). However, when observed, these circumstellar disks generally have dimensions of at most a few tenths of parsecs, masses of $M \sim 100\ M_\odot$ or less, and are generally associated with low-mass star formation. A search of the literature finds three sources, K3-50A, G10.6−0.4, and V645 Cyg, with cloud properties similar to NGC 6334A; i.e., large ($r \sim 1$ pc), massive ($M \sim 10^3\ M_\odot$), rotating disks. K3-50A, like NGC 6334A, is a shell-like H II region (Turner & Matthews 1984) with fainter radio emission extending to the northwest and southeast (De Pree et al. 1994, and references therein). K3-50A lies at the center of a large ($d \sim 1$ pc, $M \sim 2 \times 10^3\ M_\odot$) molecular cloud (Vogel & Welch 1983) which rotates about an axis parallel to the extended radio emission. Ho, Terebey, & Turner (1994) found a massive ($M \sim 10^3\ M_\odot$), rotating molecular core in G10.6−0.4. This core is more

compact (0.3 × 0.1 pc) and more flattened than the disks associated with NGC 6334A or K3-50A, but the mass estimate is similar. The case for a $10^3\ M_\odot$ rotating disk in V645 Cyg is less secure. There is some controversy concerning the correct distance to V645 Cyg, 3–6 kpc, which affects the estimates of the mass and size of the molecular gas structure. The molecular outflow from V645 Cyg is oriented north-south at small scales (15″; Torrelles et al. 1987) but appears oriented northwest-southeast at scales of 1′ and higher (Torrelles et al. 1987; Schulz et al. 1989). The ambient molecular gas at V645 Cyg is flattened east-west in the isotopic lines (^{13}CO $2 \rightarrow 1$, Torrelles et al. 1987; ^{13}CO and C^{18}O $1 \rightarrow 0$, Verdes-Montenegro et al. 1991). The ^{13}CO and C^{18}O $1 \rightarrow 0$ position-velocity diagrams also show an east-west velocity gradient (Verdes-Montenegro et al. 1991). The elongation of the ambient gas and the velocity gradient perpendicular to the small scale molecular outflow are suggestive of a large ($\geq 1.1 \times 0.5$ pc, Verdes-Montenegro et al. 1991) rotating molecular disk. The mass estimate for the disk ranges from $\geq 140\ M_\odot$ (Verdes-Montenegro et al. 1991) to $2 \times 10^3\ M_\odot$ (Torrelles et al. 1987).

Vogel & Welch (1983) first argued that the molecular disk of K3-50A might be a rotating protocluster. We suggest that these large, massive, rotating disks may, in fact, represent a common phase in the formation of open clusters. These molecular disks are well matched to the size and mass of open clusters. Open clusters generally have masses of $M_{\rm cluster} \sim 250\ M_\odot$ (Binney & Tremaine 1987), which would require a typical star formation efficiency of $\sim 10\%$ for a $2000\ M_\odot$ cloud. The molecular disks are smaller than the open clusters by approximately a factor of 2 ($r_h \sim 2$ pc), but this may be due to dynamical relaxation of the system with time.

The fact that a number of these large disks have now been discovered suggests the following mechanism for the formation of open clusters. A slowly rotating molecular cloud fragment flattens because of its angular momentum (and possibly its magnetic field). An O star condenses in the center near the rotation axis, where angular momentum effects are minimized. An H II region forms, but the stellar radiation and the expansion of the H II region are inhibited in the plane of rotation by the presence of the surrounding disk. The radiation from the massive young star can escape easily in the polar direction. This leads to the formation of two lobes of extended continuum emission perpendicular to the confining disk or torus of molecular gas and dust. If the stellar rotation axis is the same as that of the disk, and the stellar outflow is directed poleward, the surrounding molecular gas and dust may not be immediately dispersed. Turbulence in the cloud fragment or shock waves from stellar winds may induce further star formation within the disk. This additional star formation, which propagates from the center outward, then leads to a gravitationally bound star cluster.

The regions around NGC 6334A and K3-50A fit this scenario extremely well. In NGC 6334A, the H II region has a shell-like morphology with fainter radio continuum emission extending in bipolar lobes away from the shell. The H II region is surrounded by a large, massive disk of molecular gas which rotates about an axis parallel to the extended continuum lobes. NGC 6334A is at the kinematic center of the disk, which is where the first massive star is expected to form. The two protostar candidates, IRS 20 and the H_2O maser, lie at the periphery of the radio shell, as if their formation was triggered by a shock from NGC 6334A. The third NH_3 clump lies further away from NGC 6334A and is apparently not (yet) an active star formation site. Thus, the star formation activity has moved outward from NGC 6334A to IRS 20 and the H_2O maser but has not yet spread throughout the molecular disk. K3-50A also has faint, bipolar radio continuum lobes which extend from a shell-like H II region. Perpendicular to the lobes, a massive disk of molecular gas rotates around the H II region. The radio flux density is consistent with a late O star but is too low to account for the infrared luminosity $L_{\rm IR} \approx 2 \times 10^6\ L_\odot$ from the cloud. This suggests that the disk around K3-50A, like NGC 6334A, contains additional energy sources, that is, protostars.

There remain a number of difficulties in this scenario of cluster formation. First, open clusters do not seem to rotate. This implies that the rotation of the disk must be slowed in some way. As Vogel & Welch (1983) suggest, when the gas from which the cluster formed disperses, the cluster will expand. As it expands, the rotational velocity will decrease. Additionally, if the open cluster forms in the inner part of the disk, angular momentum is minimal. Second, there is the question of star formation efficiency [SFE = $M_{\rm stars}/(M_{\rm stars} + M_{\rm gas})$]. High-mass star-forming regions such as NGC 6334 tend to have efficiencies of $\sim 5\%$ or less. The SFE needed to form a gravitationally bound cluster is of order 50% (Lada & Lada 1991). However, if one considers only the gas involved in massive star formation (that is, the disk), and not the entire cloud (the NGC 6334 complex) as is usually done, the SFE rises significantly. Further, it has been suggested (e.g., Bally & Lada 1991) that the birth of an O star marks the beginning of the end of star formation because of its disruptive influence on a cloud core. If the expansion of the H II region is inhibited by a molecular disk though, star formation may not be halted. These two effects may combine to raise the SFE within these molecular disks to an efficiency consistent with a bound cluster despite the presence of an O star. Finally, even if such protocluster disks are indeed common, they may be difficult to find. The distinctive edge-on geometry of the disks and bipolar continuum emission in NGC 6334A and K3-50A led to their discovery. If a cluster is forming in a disk which is face-on, the disk would not be easily recognized. A search for bipolar H II regions might result in additional candidates. The molecular gas around these sources could then be examined for evidence of rotating disks.

7. CONCLUSIONS

1. We have found a massive ($M \sim 2 \times 10^3\ M_\odot$), flattened (2.2 × 0.9 pc) structure of molecular gas centered on the H II region NGC 6334A. This disk or torus of gas and dust is rotating at an angular velocity of $\omega \sim 2.4$ km s^{-1} pc^{-1} about a north-south axis, which is parallel to the extended continuum emission. The molecular disk is responsible for confining the H II region in the east-west direction, as suggested by RCM88. The radiation from the H II region can thus only escape perpendicular to the disk, to the north and south, and thus forms the radio and infrared continuum lobes.

2. We performed single-component model calculations of non-LTE CO excitation to determine the physical conditions of the molecular gas. Comparison of the CO bright-

ness temperatures and integrated intensity ratios with the excitation models show that the disk gas is warmer and denser ($T_k \approx 60$ K, $n \approx 3000$ cm^{-3}) than the gas to the north and south ($T_k \approx 50$ K, $n \approx 400$ cm^{-3}). As RCM88 predicted, the column density toward the continuum lobes is less than that toward the disk.

3. NH_3 and CS emission, which trace dense molecular gas, peak at the infrared source IRS 20, west of the H II region NGC 6334A. IRS 20 has a high IR luminosity with no radio continuum and coincides with a warm, dense clump of molecular gas. A second clump of NH_3 coincides with the position of an H_2O maser and the center of a CO outflow. The most likely explanation for these phenomena is that IRS 20 and the H_2O maser spot are protostars. A third NH_3 clump, west of IRS 20, has not yet formed a young stellar object but is likely to be the next site of star formation activity in the region.

4. The molecular disk centered on NGC 6334A joins K3-50A, G10.6−0.4, and V645 Cyg as the fourth example of a large, massive, rotating disk. The similarities in molecular and continuum properties between NGC 6334A and K3-50A (i.e., the massive rotating molecular disk and the perpendicular bipolar continuum emission) are remarkable. We suggest that such these massive, rotating disks provide natural environments for the formation of open clusters.

We are grateful to K. Mead for making the CO $1 \rightarrow 0$ observations, K. Janes for helpful discussions of open clusters, and to an anonymous referee for useful suggestions in clarifying the manuscript. K. E. K. was supported in part by the Clare Booth Luce Fellowship program and a Grant-in-Aid of Research from the National Academy of Sciences through Sigma Xi, The Scientific Research Society. This work was supported in part by NASA grant NAG 5-2643. Partial support for travel to the CSO was provided by the Caltech Submillimeter Observatory. This research has made use of NASA's Astrophysics Data System Abstract Service.

REFERENCES

Bally, J., & Lada, E. 1991, in ASP Conf. Ser. 13, The Formation and Evolution of Star Clusters, ed. K. Janes (San Francisco: ASP), 35
Binney, J. J., & Tremaine, S. 1987, Galactic Dynamics (Princeton: Princeton Univ. Press)
Bohigas, J. 1992, Rev. Mexicana Astron. Astrofiz., 24, 121
Boss, A. P. 1987, Proc. from the Summer School on Interstellar Processes, ed. D. Hollenbach & H. Thronson (Dordrecht: Reidel), 321
Combes, F. 1991, AR&A, 29, 195
De Pree, C. G., Goss, W. M., Palmer, P., & Rubin, R. H. 1994, ApJ, 428, 670
De Pree, C. G., Rodríguez, L. F., Dickel, H. R., & Goss, W. M. 1995, ApJ, 447, 220
Dickel, H. R., Dickel, J. R., & Wilson, W. J. 1977, ApJ, 217, 56
Flower, D. R., & Launay, J. M. 1985, MNRAS, 214, 271
Frerking, M. A., Langer, W. D., & Wilson, R. W. 1982, ApJ, 262, 590
Garay, G., & Rodríguez, L. F. 1990, ApJ, 362, 191
Gyulbuaghian, A. L., Glushkov, Y. I., & Denisyuk, E. 1978, ApJ, 224, L137
Harvey, P. M., & Gatley, I. 1983, ApJ, 269, 613 (HG83)
Harvey, P. M., Hyland, A. R., & Straw, S. M. 1987, ApJ, 317, 173
Ho, P. T. P., Terebey, S., & Turner, J. L. 1994, ApJ, 423, 320
Jackson, J. M., Paglione, T. A. D., Carlstrom, J. E., & Rieu, N.-Q. 1995, ApJ, 438, 695
Kraemer, K. E., & Jackson, J. M. 1997, in preparation
Kraemer, K. E., Jackson, J. M., Paglione, T. A. D., & Lane, A. P. 1994, in ASP Conf. Ser. 73 From Gas to Stars to Dust, ed. M. R. Haas, J. A. Davidson, & E. F. Erickson (San Francisco: ASP), paper 107
Lada, C. J., & Lada, E. 1991, The Formation and Evolution of Star Clusters, ed. K. Janes (San Francisco: ASP), 3
Loughran, L., McBreen, B., Fazio, G. G., Rengarajan, T. N., Maxson, C. W., Serio, S., Sciortino, S., & Ray, T. P. 1986, ApJ, 303, 629
McBreen, B., Fazio, G. G., Stier, M., & Wright, E. L. 1979, ApJ, 232, L183
Mestel, L. 1965, Quart. QJRAS, 6, 161
Moran, J. M., & Rodríguez, L. F. 1980, ApJ, 236, L159
Neckel, T. 1978, A&A, 69, 51
Panagia, N. 1973, AJ, 78, 929
Phillips, J. P., de Vries, C. P., & de Graauw, T. 1986, ApJS, 65, 465
Rodríguez, L. F., Cantó, J., & Moran, J. M. 1982, ApJ, 255, 103
———. 1988, ApJ, 333, 801 (RCM88)
Rodríguez, L. F., Moran, J. M., Ho, P. T. P., & Gottlieb, E. W. 1980, ApJ, 235, 845
Schulz, A., Black, J. H., Lada, C. J., Ulich, B. L., Martin, R. N., Snell, R. L., & Erickson, N. J. 1989, ApJ, 341, 288
Shu, F., Najita, J., Galli, D., Ostriker, E., & Lizano, S. 1993, Protostars & Planets Vol. 3, ed. E. H. Levy & J. I. Lunine (Tucson: Univ. Arizona Press), 3
Stutzki, J., & Winnewisser, G. 1985, A&A, 144, 13
Torrelles, J. M., Anglada, G., Rodríguez, L. F., Cantó, J., & Barral, J. F. 1987, A&A, 177, 171
Torrelles, J. M., Rodríguez, L. F., Cantó, J., Carral, P., Marcaide, J., Moran, J. M., & Ho, P. T. P. 1983, ApJ, 274, 214
Turner, B. E., & Matthews, H. E. 1984, ApJ, 277, 164
Ulich, B. L., & Haas, R. W. 1976, ApJS, 30, 247
Verdes-Montenegro, L., Gómez, J. F., Torrelles, J. M., Anglada, G., Estalella, R., & López, R. 1991, A&A, 244, 84
Vogel, S. N., & Welch, W. J. 1983, ApJ, 269, 568